Langmuir

ARTICLE

pubs.acs.org/Langmuir

Self-Assembly of Gold Nanorods into Symmetric Superlattices Directed by OH-Terminated Hexa(ethylene glycol) Alkanethiol

Yong Xie,[†,‡] Shengming Guo,[‡] Yinglu Ji,[§] Chuanfei Guo,[‡] Xinfeng Liu,[∥] Ziyu Chen,[†] Xiaochun Wu,[*,§] and Qian Liu[*,‡]

[†]Department of Physics, Beijing University of Aeronautics and Astronautics, Beijing 100191, China

[‡]Laboratory for Nanodevices, National Center for Nanoscience and Technology, Beijing 100190, China

[§]Key Laboratory of Standardization and Measurement for Nanotechnology, Chinese Academic of Sciences, Beijing 100190, China

[∥]School of Physical and Mathematical Sciences, Nanyang Technological University, 637371 Singapore

Supporting Information

ABSTRACT:

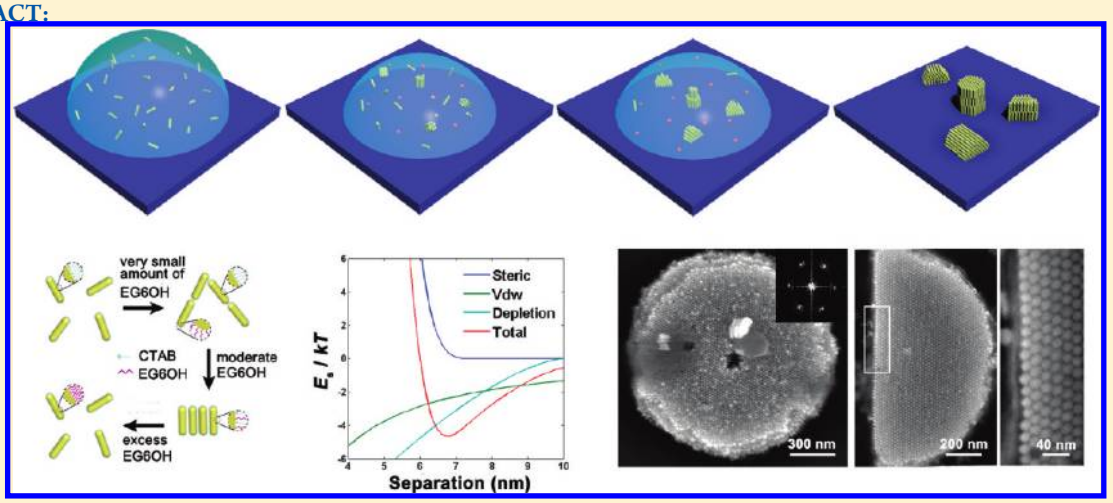

The self-assembly of anisotropic gold nanorods (GNRs) into ordered phases remains a challenge. Herein, we demonstrated the fabrication of symmetric circular- or semicircular-like self-assembled superlattices composed of multilayers of standing GNRs by fine-tuning the repulsive interactions among GNRs. The repulsive force is tailored from electrostatic interaction to steric force by replacing the surface coating of cetyltrimethylammonium bromide (CTAB) (ζ potential of 20−50 mV) with an OH-terminated hexa(ethylene glycol) alkanethiol (here termed as EG_6OH, ζ potential of −10 mV). The assembly mechanism is discussed via theoretical analyses of the major interactions, and an effective balance between the repulsive steric and attractive depletion interactions is the main driving force for the self-assembly. The real-time observations of solution assembly (UV−vis−NIR absorption spectroscopy) supports the mechanism that we suggested. The superlattices obtained here not only enrich the categories of the self-assembled structures but more importantly deepen the insight of the self-assembly process and pave the way for various potential applications.

INTRODUCTION

A variety of self-assembled colloidal nanoparticles may function as metamaterials, biosensors, and even nanodevices.[1−4] In the last 5 years, the self-assembly of nonspherical nanoparticles has become popular because such structures can stimulate some anisotropic optical and electrical properties and meet the needs of many practical applications.[5−10] Gold nanorods (GNRs), as one kind of shape- and size-dependent plasmonic building block, are very suitable for exploiting the self-assembled superstructures. Solvent evaporation has been widely recognized as a simple and effective strategy for assembling GNRs into ordered phases (nematic or smectic) that are based on far-from-equilibrium effects such as fluid convection and leads to so-called "coffee ring" patterns.[6,11,12] With the effects, most of the GNRs are transferred and assembled into the ordered phases at the ring (or at the droplet edge). Away from the ring, an ordered arrangement of the remaining GNRs is seldom observed. However, an advantage is that the internal region of the drying droplet can create a near-equilibrium status, especially during the final stage of drying under the condition of slow evaporation.[13,14] Such a near-equilibrium

Received: June 21, 2011
Revised: August 9, 2011

   dx.doi.org/10.1021/la202320k | *Langmuir* XXXX, XXX, 000–000

status can promote the formation of GNR self-assemblies because each free rod can easily find its most stable position in the solution. Besides, the formation of the self-assemblies needs a balance of effective repulsive interactions and attractive interactions among the nanoparticles.[15,16] In the case of cetyltrimethylammonium bromide (CTAB)-stabilized GNRs, the strong electrostatic forces need to be reduced. A conventional approach is to adjust the ionic strength of the surrounding solution. However, the introduction of free ions always inevitably brings about negative effects, typically salt crystallization, that seriously deteriorate the formation of the self-assemblies. Alternatively, the use of a weak polar OH-terminated hexa(ethylene glycol) alkanethiol (EG_6OH), which binds to the GNRs surface by a strong Au−S bond, can reduce the long-range electrostatic repulsion, and a sufficient dose of the EG_6OH thiol can also prevent the GNRs from random aggregation owing to a repulsive steric force.[17] The effective scope of the steric force is not beyond the scale of the totally stretched EG_6OH molecules (about 4 nm). Such a short-range repulsive force is desirable against the attractive force for the formation of GNR self-assemblies. The attractive force causes the particles to come close to each other, and the short-range repulsive force serves to stabilize the particles within a certain distance and then directs the GNRs into ordered phases. In this article, through tailoring the relatively large electrostatic interaction to a "softer" steric force using thiolated EG_6OH, symmetric circular- or semicircular-like self-assembled superlattices composed of multilayers of standing GNRs are obtained under slow evaporation. Very recently, such 3D GNR superlattices have been found to be a highly active surface-enhanced Raman scattering (SERS) substrate for the fast, sensitive detection of certain biological molecules in complex biological media.[18]

EXPERIMENTAL SECTION

Materials. OH-terminated hexa(ethylene glycol) undecanethiol ($HS(CH_2)_{11}(OCH_2CH_2)_6OH$, termed EG_6OH, CAS registry number 130727-44-5)[19] was purchased from ProChimia. CTAB was purchased from Amresco. All other chemicals used in the experiments were purchased from Sigma-Aldrich without further purification.

Preparation of GNRs. CTAB-coated GNRs were synthesized by a well-developed seed-mediated growth method.[20,21] Rods with an average aspect ratio of 3.5 (length ≈ 60 nm, diameter ≈ 17 nm) were used as building blocks. After synthesis, GNRs were centrifuged (9000 rpm, 30 °C for 7 min) and redispersed in deionized water (18 MΩ·cm) to a concentration of 0.5 nM with a CTAB concentration of 1.0 mM, where the concentration of the GNRs was determined by the Beer−Lambert law, $A = \varepsilon cl$, with a molar extinction coefficient of $\varepsilon = 4.6 \times 10^9\ M^{-1}\ cm^{-1}$ from ref 22.

Preparation of EG_6OH Thiol-Coated GNRs. One milliliter of the GNR solution was centrifuged for the second time (9000 rpm, 30 °C for 7 min). After the removal of as much of the supernatant as possible, the precipitate (about 10 μL) was diluted to 1 mL with deionized water and then mixed with the EG_6OH solution (10 mM, 200 μL). The mixture was put into a 30 °C water bath to react for 4 h, guaranteeing a saturation adsorption of EG_6OH molecules on the GNRs. The final rod concentrations were adjusted to 5, 15, 25, and 35 nM (ultrasonic bath for 1 min) for self-assembly.

Formation of Self-Assembled Superlattices. Fifteen microliters of the concentrated GNR solution was dropped onto a clean silicon wafer for slow evaporation at 25 °C with an environmental humidity of 50 ± 5%.

SEM and TEM Imaging. Scanning electron microscope (SEM) images of the samples were acquired with a Hitachi S-4800 microscope operating at 10 kV for secondary electron imaging (SEI). The assembled geometry of the GNRs was determined from the SEM images both directly from each image and from the fast Fourier transform of the corresponding SEM image. The transmission electron microscope (TEM) images of the samples were acquired with a Tecnai G2 20 S-TWIN microscope operating at an acceleration voltage of 200 kV.

Observations of GNR Self-Assemblies in Solution. The effect of EG_6OH thiol concentrations on the GNR self-assemblies was investigated by real-time UV−vis−NIR spectra, which were recorded on a UV−vis−NIR spectrophotometer (Cary50) under the following scan conditions: the wavelength is 200−1100 nm, the scan rate is 600 nm min^{-1}, the temperature is 25 °C, and the cuvette is 1 cm × 1 cm quartz colorimetric ware. The measured samples were prepared as follows: twice-centrifuged GNRs (1 mL, ∼0.5 nM) were diluted to 3 mL in advance. Different amounts of EG_6OH thiols (0.5−500 μL, 1 mM) were pipetted into the test GNRs solution.

Scattering Spectroscopy Measurements. Microarea scattering spectroscopy measurements were performed on an Olympus BX51 confocal microscope integrated with a monochromator (SP2300i) and liquid-N_2-cooled charge-coupled detector (CCD) (Princeton Instruments, Spec 10). The scattering spectra were collected with an LMPlanFl dark-field objective lens (50×, NA = 0.50) and focused onto the entrance slit of the monochromator for the spectroscopy. A 100 W quartz−tungsten−halogen lamp was used as the white-light illumination. The confocal area (∼1 μm in diameter) was located on the region of the superlattice by using a pinhole (10 μm in diameter) in the collecting optical path. The scattering spectra from the superlattice were corrected by subtracting the background spectra collected from the nearby regions containing no particles.

RESULTS AND DISCUSSION

The droplet evaporation method generally leads to the formation of a "coffee ring" as shown in Figure S1a. In the ring region, a dense nematic arrangement of the GNRs is observed as reported previously. Away from the region, islandlike assemblies with circular- and semicircular-like geometries, which we discuss in this article, are observed from the low-magnification SEM image (Figure 1a). These symmetric geometries have an average diameter of 1.5 μm and randomly scatter on the substrate. The statistical data show (Figure 1a inset) that the circular-like geometries have a yield of ∼19% and the semicircular-like geometries occupy the majority. Further observations present (Figure 1b) many "superlattice" structures composed of thousands of neatly arranged, individual GNRs. The so-called superlattice here is a type of generalized configuration that is similar to the atomic lattice in terms of the periodic arrangement of the basic units.[10,23,24] Figure 1c shows a typical circular-like superlattice that has a diameter of 1.3 μm and possesses hexagonal symmetry as shown by the fast Fourier transform (FFT) of the corresponding SEM image. Figure 1d shows a typical semicircular-like superlattice with a diameter of 1.2 μm. The side view of the semicircular superlattice presents a clear layered array (Figure S1c in Supporting Information). Interestingly, the semicircular superlattices often have a sharp edge. Figure 1e demonstrates that the GNRs within the edge arrange almost along a straight line and maintain a constant separation of about 6 nm between adjacent rods. For an explanation of the sharp edges, we suggest that they should result from the substrate confinement based on the following reasons: (1) the edges are impossible to form on an air−water interface because of the strong convection and caused a perturbation;[13] (2) none of the edges are found to face upward (Figure S2 in Supporting Information); (3) there are many tiled

dx.doi.org/10.1021/la202320k |Langmuir XXXX, XXX, 000–000

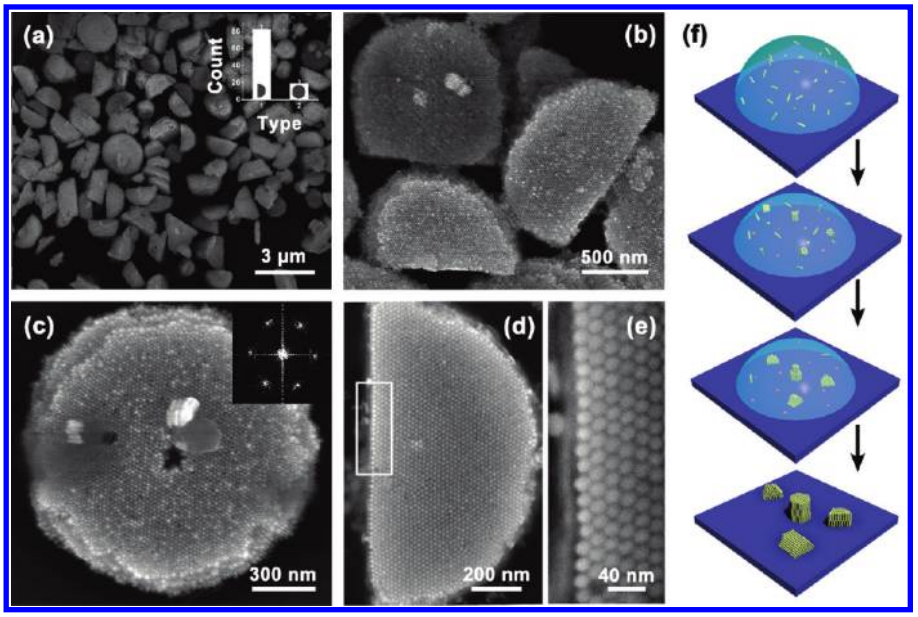

Figure 1. SEM images of the circular- or semicircular-like self-assembled superlattices obtained by EG_6OH-coated GNRs. (a) SEM image of the self-assemblies. The inset shows the statistical data of the circular- and semicircular-like geometries in the image. The error bars represent the standard deviations of the statistical results. (b) High-magnification SEM image of the self-assemblies. (c) High-magnification SEM image of a circular-like GNR superlattice. The inset image is the fast Fourier transform of the image in panel c, suggesting good hexagonal symmetry. (d) High-magnification SEM image of semicircular-like GNR superlattices. (e) SEM image clearly showing the sharp edge in panel d. (f) Evolution of the symmetric superlattices in different stages of droplet drying, showing the initial dispersion of the GNRs in the aqueous solution, the nucleation of the assemblies, the growth process of the assemblies, and the formation of the sharp edges and the final formation of the superlattices. The pink dots in the sketches represent the EG_6OH micelles.

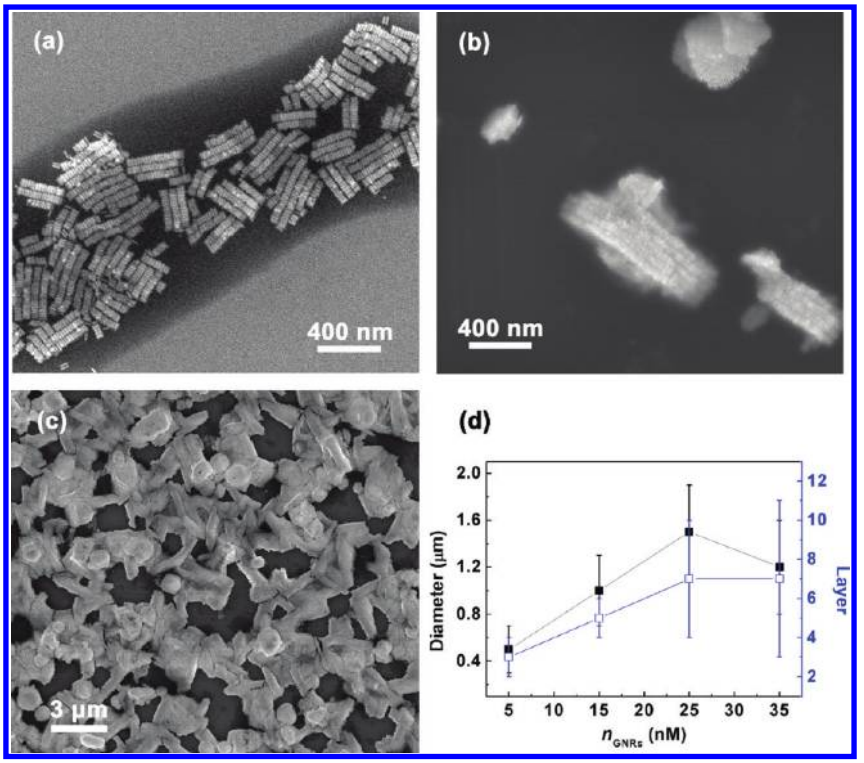

Figure 2. Effect of GNR concentration on the growth of the superlattice. (a) Typical morphologies at a GNR concentration of 5 nM. Tens of individual GNRs are arranged in a few rows with an average length of 400 nm. (b) Morphologies at a concentration of 15 nM showing a typical striplike superlattice with about five layers. (c) Morphologies at a concentration of 35 nM. Some circular-like superlattices are found with a diameter of 1.2 μm covering the massive self-assembled structures. (d) Dependence of the diameter and layer number of the superlattices on the GNR concentrations. The error bars represent standard deviations of the statistical diameters and layers.

dx.doi.org/10.1021/la202320k |*Langmuir* XXXX, XXX, 000–000

superlattices with edges tightly adhering to the substrate (Figure S3 in Supporting Information). From these, a specific evolution of the superlattices can be speculated: the nucleation of the assemblies should occur within the solution by suitable rod interactions during the final stage of droplet drying. Once the initial nucleus is formed, free rods will assemble around the nucleus, leading to the growth of the assemblies. Considering the axial symmetry of the GNRs themselves, we believe that the initial nuclei have hexagonal symmetry in a side-by-side mode. After that, the sedimentation will be followed because of the increasing gravity of the assemblies. If the nuclei lie down on the substrate, then the growth of the assemblies in the direction of substrate is inhibited and an edge as smooth as the substrate is formed. In contrast, if the nuclei stand up on the substrate, then the circular superlattices can be formed (Figure 1f). Also, the circular or semicircular symmetry of the superlattices is subjected to the surface energy minimum.[25] For the reason that the nuclei have a larger contact area with respect to the substrate by lying down, the probability of semicircular-like superlattices is higher than that of circular-like ones. This agrees with our statistical results: the probability of obtaining a semicircular-like superlattice is about 4 times that of obtaining a circular-like superlattice (Figure 1a and Figure S1b in the Supporting Information).

On account of the influence of the GNR concentrations on the self-assemblies,[26] we study the growth rhythm of the symmetric superlattices under different GNRs concentrations. First, at low concentrations (no more than 5 nM), some side-by-side (SS) arrays are observed (Figure 2a) with a persistent length of 0.5 μm and a width of 0.2 μm (about three layers of standing rods). The arrays are very likely to be early prototypes of the superlattices. Second, at a medium GNR concentration of 15 nM, some self-assemblies are found with a diameter of 1 μm and a layer numbers of five (Figure 2b) on average, indicating that the superlattices have formed but without sufficient growth. Third, when the concentration reaches to a high value of 25 nM, many circular- or semicircular-like self-assembled superlattices are observed with a diameter of 1.5 μm and a layer number of seven (Figure 1) on average. Hence, a roughly linear growth of superlattices is obtained by plotting the dependence of the diameter and layer number of the superlattices on the GNR concentration as shown in Figure 2d. However, with further increases in the GNR concentration to an extremely high value of about 35 nM, the self-assemblies are observed to stack together and form large, cross-linked 3D structures with some circular-like superlattices on them (Figure 2c). As a result, the linear growth reaches its maximum and an optimal GNR concentration of 25 nM is confirmed for the formation of the symmetric superlattices.

In this section, we discuss the SS assembly mechanism of the superlattices by analyzing the interactions among the GNRs. Generally, CTAB-coated GNRs do not easily form self-assemblies because of the large electrostatic repulsion (ζ potential of 20−50 mV).[10] Instead of CTAB, the use of the EG_6OH surfactant significantly reduces the repulsion (ζ potential of −10 mV, Figure S4 in the Supporting Information). Considering the weak dissociation of the EG_6OH molecules in the aqueous solution[27] and the low CTAB concentrations used in the experiments, the screening effect of the electrical double layer (EDL) on the GNR surface charge is not obvious.[28] Directly approximating −10 mV as the surface potential of two parallel GNRs and using the electrostatic force data calculated with Ansoft Maxwell software (Figure S5 in the Supporting Information), we fit a simple exponential equation of $E_0 \exp(-x/\kappa)$ with $E_0 \approx 1\ kT$ and

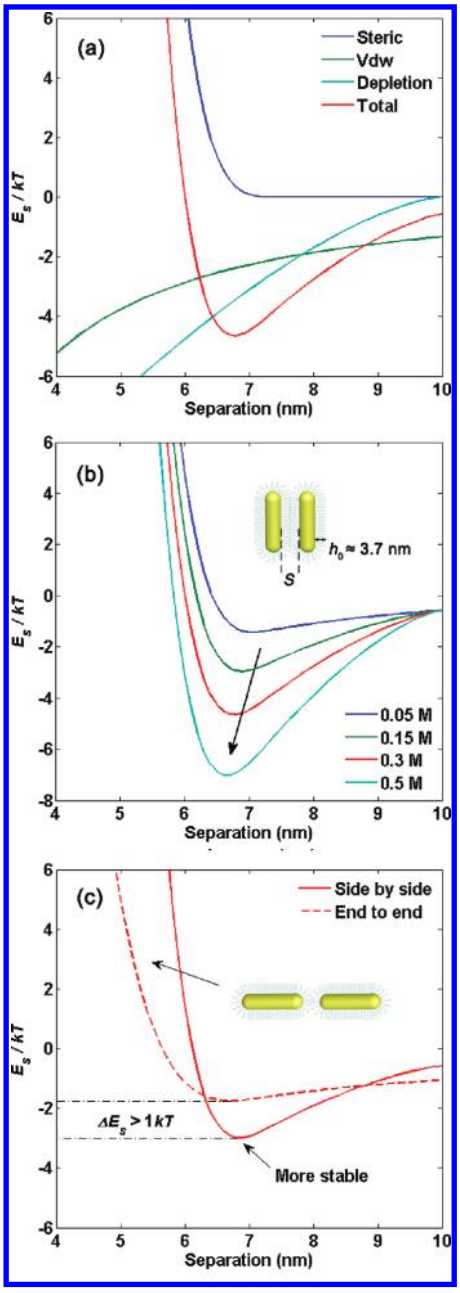

Figure 3. Theoretical calculation results for the self-assemblies. (a) Typical potential curves for parallel configurations with a separation x of two GNRs. (b) Total potential curves of different EG_6OH concentrations for two parallel GNRs. The inset shows a schematic diagram of the two parallel GNRs coated with EG_6OH. (c) Total potential curves of the end-to-end configuration (---) and the side-by-side configuration (−) under the same conditions. The inset shows a schematic diagram of the end-to-end GNRs coated with EG_6OH.

$\kappa \approx 40$ nm. And a maximum electrostatic energy of about 1 kT is given. This means that the electrostatic interaction in this situation cannot stabilize the free GNRs. However, when the rods meet at a distance of several nanometers, they again have to bear a repulsive steric force, which creates between two surfaces upon compression of neighboring EG_6OH brushes.[29] The steric force increases with the increase in EG_6OH concentration owing to the high grafting density and the large Flory radius of the EG_6OH molecules. Because the van der Waals attraction cannot

dx.doi.org/10.1021/la202320k |*Langmuir* XXXX, XXX, 000–000

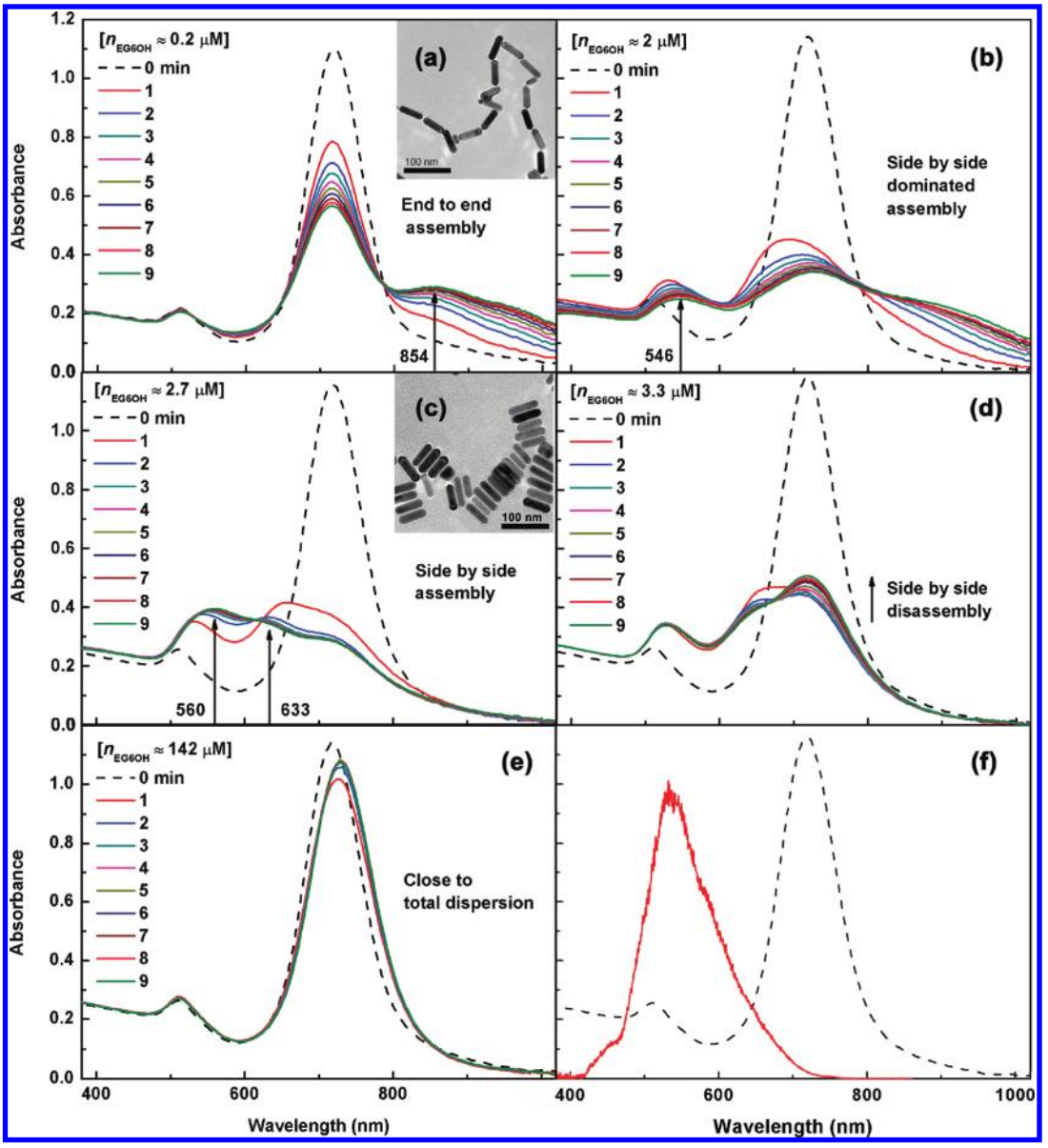

Figure 4. Results of real-time UV−vis−NIR spectra and a microscattering spectrum. (a) Kinetic spectra measurement of the GNR solution with an EG_6OH concentration of 0.2 μM. The dashed line shows the spectral result prior to the addition of EG_6OH. The inset TEM image shows the corresponding self-assembly morphology in the solution. (b) EG_6OH concentration of 2 μM. A assembly peak is observed at a wavelength of 546 nm, suggesting the side-by-side-dominated assembly. (c) EG_6OH concentration of 2.7 μM. Two clear assembly peaks are observed at 560 and 633 nm. The inset TEM image is the corresponding self-assembly morphology. (d, e) EG_6OH concentrations of 3.3 and 142 μM, respectively. Disassembly is observed. (f) Scattering spectrum of the circular-like superlattice collected with a confocal microscope under while-light illumination.

balance the steric repulsion at a certain EG_6OH concentration, the GNRs disperse well in the solution.[17,30] Next, as the EG_6OH concentration further increases to a higher value, the EG_6OH molecules aggregate spontaneously to form large micelles.[31] An attractive depletion force will become significant because of the enhanced depletion of micelles from the space between the GNRs.[8,32] Hence, we determine that interactions among the steric, van der Waals, and depletion force should be the major ones responsible for the self-assembly of the GNRs. In the case of two parallel rods (Figure 3b inset), the total interaction potentials are calculated (Theoretical Calculations section in the Supporting Information).[17,29,31−33] Figure 3a shows the results in which the most stable separation is about 6.8 nm with a minimum energy of $-4.6kT$. This indicates that although the steric repulsion generates a large potential barrier at separations of less than 7 nm, the depletion attraction can effectively reduce the barrier and forms a potential well. With the increase in the EG_6OH concentration, the depletion attraction proportionally increases, leading to a deepening potential well and a decreasing separation as shown in Figure 3b, which means that the SS assembly of the GNRs is enhanced. Therefore, the attractive force that balances the steric force for the self-assembly is mainly the depletion force. As a comparison, we also calculate the total energy of the end-to-end (EE) configuration (Figure 3c inset). Compared with the potentials of the two configurations, it can be determined that the SS assembly of the GNRs is more stable than the EE assembly

dx.doi.org/10.1021/la202320k |*Langmuir* XXXX, XXX, 000–000

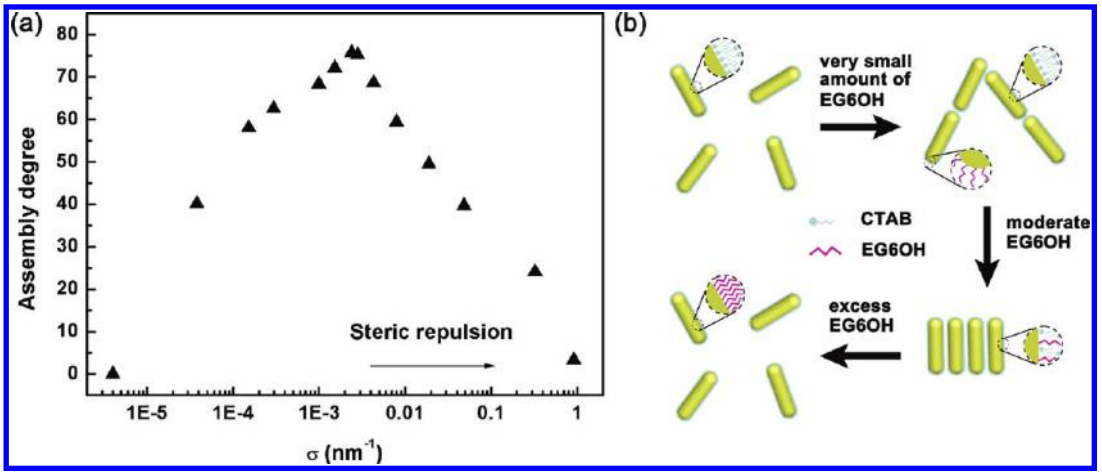

Figure 5. Effect of EG_6OH spatial distribution and coverage on solution assembly. (a) Relationship of the GNR degree of assembly and EG_6OH grafting density. The grafting density is obtained from the EG_6OH concentrations on the basis of the relation $\sigma \approx an^{3/2}$.[42] A final grafting density of 1 chain per nm^2 is assumed. (b) Schematic diagram representing the transformation of the self-assembled morphologies as well as the selective adsorption of EG_6OH molecules.

because of the lower minimum energy. An energy gap of about 1 kT is obtained as shown in Figure 3c. Therefore, it can be concluded that the formation of the SS assembly in the superlattices should be attributed to the balance of the depletion attraction and the short-range steric repulsion.

To verify the above theoretical analyses and gain more insight into the main interactions responsible for the assemblies, we further investigated the effects of the EG_6OH spatial distribution and coverage on the interactions and thereby induced in-solution assemblies. The CTAB concentration in the GNR solution is about 3 μM after two centrifugations. When adding a small amount of EG_6OH (about 0.2 μM) to the GNR solution, we observed an obvious EE assembly that was due to the appearance of a broad absorption band in the longer-wavelength region as shown in Figure 4a. In contrast, the transverse surface plasmon resonance (TSPR) band shows no obvious change. The TEM image verified the EE assembly mode. The ζ potential of the GNR assemblies is about 10 mV, which is lower than that of the pure CTAB-coated GNRs (about 17 mV, Figure S4 in the Supporting Information). For the EE assembly at the lower EG_6OH concentration, the EG_6OH molecules are mainly bound to the end facets of GNRs via the Au−S bond and the side facets of the GNRs are still bound by the CTA^+ headgroup. Because of opposite electrostatic properties of the two surfactants, the electrostatic repulsion of the end facets is reduced and the van der Waals force induces the EE assembly.[34−38] When the EG_6OH concentration is increased to 2 μM as shown in Figure 4b, the SS assembly becomes dominate because the change in the shorter-wavelength region (around the TSPR) is more obvious than that in the longer-wavelength region. The transition from EE to SS mode can be regarded as the beginning of a substitution process (Figure S6 in the Supporting Information, i.e., the EG_6OH molecules gradually displace the CTAB molecules on the side facets of the GNRs because of the stronger ligand bond between Au and S, thus the SS mode can be triggered).[39,40] As the EG_6OH concentration reaches 2.7 μM, the neat SS mode dominates with two assembled bands that peak at 633 and 560 nm, corresponding to LSPR and TSPR, respectively (Figure 4c). A corresponding TEM image confirms the SS assembly mode. The ζ potential measurements in this range demonstrate a continuous decrease from 4 to −10 mV, indicating more EG_6OH on the surfaces of the rods. By further increasing the EG_6OH concentration to 3.3 μM, the SS mode still dominates but the degree of assembly is reduced as the intensity of the monomers (720 nm) increases (Figure 4d). At a relatively high value of 142 μM, the GNRs do not assemble anymore. Meanwhile, the ζ potential is stabilized at about −10 mV. This means that the substitution of EG_6OH with CTAB has reached saturation. By plotting the dependence of the degree of assembly on the EG_6OH degree of coverage (characterized by the grafted density σ), we found that the degree of assembly first increases, then reaches maximum, and finally decreases with the degree of coverage, showing a "ridge shape" dependence (Figure 5a).[41] Here, the degree of assembly is defined by the relative change in the monomer's absorbance at 720 nm as $\mathrm{deg}(k) = (\mathrm{Abs}(k_0) - \mathrm{Abs}(k))100/\mathrm{Abs}(k_0)$, where $\mathrm{Abs}(k_0)$ is the monomer's absorbance prior to adding EG_6OH and $\mathrm{Abs}(k)$ is the absorbance after adding EG_6OH. At higher EG_6OH concentrations, GNRs do not assemble, indicating the existence of a repulsive force. We believe that this repulsive force is a steric force. The transition of the assembly mode in different stages is attributed to the spatial distribution of EG_6OHs on the rods (Figure 5b). In addition, by further collecting the micro-scattering spectra of the circular-like superlattice, it is found that only the TSPR band is excited in the array (Figure 4f), which is further evidence of the neat SS assembly mode.

CONCLUSIONS

Through the use of an oligo(ethylene glycol) thiol (EG_6OH) surfactant, we obtained a novel self-assembled superlattice within the coffee stain by the simple droplet evaporation method. The superlattices have two typical circular- and semicircular-like shapes that are composed of multilayers of standing GNRs. The assemblies are dependent on the GNR concentration, and an optimal concentration of 25 nM is found. The theoretical analyses indicate that the neat SS assembly of the superlattices is attributed to the balance between the steric force and the depletion force generated by EG_6OH micelles. The symmetric morphology of the superlattices is attributed to the surface-energy minimum. Changes in the UV−vis−NIR absorption spectra depend sensitively on the in-solution assemblies further confirming

dx.doi.org/10.1021/la202320k |*Langmuir* XXXX, XXX, 000–000

the existence of steric force in the EG_6OH-modified GNRs. Considering the functionalities of the EG_6OH-coated surfaces (i.e., protein resistance, "cell friendly"), these symmetric self-assembled superlattices are expected to demonstrate potentials in biodetecting/biosensing and plasmonic metamaterials.

■ ASSOCIATED CONTENT

Supporting Information. SEM images of the superlattice distribution, AFM images of superlattices, tiled superlattices for determining the sharp edge and its cause, ξ potential for in-solution assembly, electrostatic force data, Raman spectra, and detailed theoretical equations and parameters used in calculations. This material is available free of charge via the Internet at http://pubs.acs.org.

■ AUTHOR INFORMATION

Corresponding Author

*E-mail: wuxc@nanoctr.cn (X.C.W.); liuq@nanoctr.cn (Q.L.). Tel: +86-10-8254-5577 (X.C.W.); +86-10-8254-5585 (Q.L.).

■ ACKNOWLEDGMENT

This work was supported by the NSFC (10974037 and 61006078), the National Basic Research Programs of China (2010CB934102 and 2011CB932802), the International S&T Cooperation Program (2010DFA51970), and the Eu-FP7 Project (no. 247644).

■ REFERENCES

(1) Stebe, K. J.; Lewandowski, E.; Ghosh, M. *Science* **2009**, *325*, 159–160.
(2) Takahashi, H.; Niidome, Y.; Niidome, T.; Kaneko, K.; Kawasaki, H.; Yamada, S. *Langmuir* **2005**, *22*, 2–5.
(3) Chen, C.-C.; Lin, Y.-P.; Wang, C.-W.; Tzeng, H.-C.; Wu, C.-H.; Chen, Y.-C.; Chen, C.-P.; Chen, L.-C.; Wu, Y.-C. *J. Am. Chem. Soc.* **2006**, *128*, 3709–3715.
(4) Philp, D.; Stoddart, J. F. *Angew. Chem., Int. Ed.* **1996**, *35*, 1154–1196.
(5) Nakashima, H.; Furukawa, K.; Kashimura, Y.; Torimitsu, K. *Langmuir* **2008**, *24*, 5654–5658.
(6) Ming, T.; Kou, X.; Chen, H.; Wang, T.; Tam, H.-L.; Cheah, K.-W.; Chen, J.-Y.; Wang, J. *Angew. Chem., Int. Ed.* **2008**, *47*, 9685–9690.
(7) Park, K.; Koerner, H.; Vaia, R. A. *Nano Lett.* **2010**, *10*, 1433–1439.
(8) Baranov, D.; Fiore, A.; van Huis, M.; Giannini, C.; Falqui, A.; Lafont, U.; Zandbergen, H.; Zanella, M.; Cingolani, R.; Manna, L. *Nano Lett.* **2010**, *10*, 743–749.
(9) Liu, J. F.; Wang, L. L.; Sun, X. M.; Zhu, X. Q. *Angew. Chem., Int. Ed.* **2011**, *49*, 3492–3495.
(10) Guerrero-Martínez, A.; Pérez-Juste, J.; Carbó-Argibay, E.; Tardajos, G.; Liz-Marzán, L. *Angew. Chem., Int. Ed.* **2009**, *48*, 9484–9488.
(11) He, J.; Zhang, Q.; Gupta, S.; Emrick, T.; Russell, T.; Thiyagarajan, P. *Small* **2007**, *3*, 1214–1217.
(12) Nobile, C.; Carbone, L.; Fiore, A.; Cingolani, R.; Manna, L.; Krahne, R. *J. Phys.: Condens. Matter* **2009**, *21*, 264013−264018.
(13) Deegan, R. D.; Bakajin, O.; Dupont, T. F.; Huber, G.; Nagel, S. R.; Witten, T. A. *Nature* **1997**, *389*, 827–829.
(14) Hu, H.; Larson, R. G. *Langmuir* **2005**, *21*, 3963–3971.
(15) Min, Y.; Akbulut, M.; Kristiansen, K.; Golan, Y.; Israelachvili, J. *Nat. Mater.* **2008**, *7*, 527–538.
(16) Li, F.; Josephson, D. P.; Stein, A. *Angew. Chem., Int. Ed.* **2011**, *50*, 360–388.
(17) Prime, K. L.; Whitesides, G. M. *J. Am. Chem. Soc.* **1993**, *115*, 10714–10721.
(18) Alvarez-Puebla, R. A.; Agarwal, A.; Manna, P.; Khanal, B. P.; Aldeanueva-Potel, P.; Carbó-Argibay, E.; Pazos-Pérez, N.; Vigderman, L.; Zubarev, E. R.; Kotov, N. A.; Liz- Marzán, L. M. *Proc. Natl. Acad. Sci. U.S.A.* **2011**, *108*, 8157–8161.
(19) Tan, J. L.; Tien, J.; Chen, C. S. *Langmuir* **2001**, *18*, 519–523.
(20) Nikoobakht, B.; El-Sayed, M. A. *Chem. Mater.* **2003**, *15* (10), 1957–1962.
(21) Gole, A.; Murphy, C. J. *Chem. Mater.* **2004**, *16*, 3633–3640.
(22) Orendorff, C. J.; Murphy, C. J. *J. Phys. Chem. B* **2006**, *110*, 3990–3994.
(23) Zhao, N.; Liu, K.; Greener, J.; Nie, Z.; Kumacheva, E. *Nano Lett.* **2009**, *9*, 3077–3081.
(24) Ciszek, J. W.; Huang, L.; Tsonchev, S.; Wang, Y.; Shull, K. R.; Ratner, M. A.; Schatz, G. C.; Mirkin, C. A. *ACS Nano* **2009**, *4*, 259–266.
(25) Dhont, J. K. G.; Smits, C.; Lekkerkerker, H. N. W. *J. Colloid Interface Sci.* **1992**, *152*, 386–401.
(26) Mitamura, K.; Imae, T.; Saito, N.; Takai, O. *J. Phys. Chem. B* **2007**, *111*, 8891–8898.
(27) Weisbecker, C. S.; Merritt, M. V.; Whitesides, G. M. *Langmuir* **1996**, *12*, 3763–3772.
(28) Walker, D. A.; Kowalczyk, B.; de la Cruz, M. O.; Grzybowski, B. A. *Nanoscale* **2011**, *3*, 1316–1344.
(29) Bishop, K. J. M.; Wilmer, C. E.; Soh, S.; Grzybowski, B. A. *Small* **2009**, *5*, 1600–1630.
(30) Pale-Grosdemange, C.; Simon, E. S.; Prime, K. L.; Whitesides, G. M. *J. Am. Chem. Soc.* **1991**, *113*, 12–20.
(31) Tanford, C. *J. Phys. Chem.* **1974**, *78*, 2469–2479.
(32) Asakura, S.; Oosawa, F. *J. Polym. Sci.* **1958**, *33*, 183–192.
(33) Russel, W. B.; Saville, U. A.; Schowalter, W. R., *Colloidal Dispersions*; Cambridge University Press: New York, 1999.
(34) Huang, X.; Neretina, S.; El-Sayed, M. A. *Adv. Mater.* **2009**, *21*, 4880–4910.
(35) Chang, J.-Y.; Wu, H.; Chen, H.; Ling, Y.-C.; Tan, W. *Chem. Commun.* **2005**, *8*, 1092–1094.
(36) Hu, X.; Cheng, W.; Wang, T. *Nanotechnology* **2005**, *16*, 2164–2169.
(37) Shibu Joseph, S. T.; Ipe, B. I.; Pramod, P.; Thomas, K. G. *J. Phys. Chem. B* **2005**, *110*, 150–157.
(38) Nie, Z.; Fava, D.; Kumacheva, E.; Zou, S.; Walker, G. C.; Rubinstein, M. *Nat. Mater.* **2007**, *6*, 609–614.
(39) Rayavarapu, R. G.; Petersen, W.; Hartsuiker, L.; Chin, P.; Janssen, H.; Leeuwen, F. W.; Otto, C.; Manohar, S.; Leeuwen, T. G. *Nanotechnology* **2010**, *21*, 145101–145111.
(40) Zhong, L. B.; Zhou, X.; Bao, S. X.; Shi, Y. F.; Wang, Y.; Hong, S. M.; Huang, Y. C.; Wang, X.; Xie, Z. X.; Zhang, Q. Q. *J. Mater. Chem.* **2011**, DOI: 10.1039/c1jm11193k.
(41) Sun, Z.; Ni, W.; Yang, Z.; Kou, X.; Li, L.; Wang, J. *Small* **2008**, *4*, 1287–1292.
(42) de Gennes, P. G. *Macromolecules* **1980**, *13*, 1069–1075.